# Revised Mechanism of C(sp<sup>3</sup>)–C(sp<sup>3</sup>) Reductive Elimination from Ni(II) with the Assistance of a Z-Type Metalloligand

Tao Zhang,<sup>†,∥,⊥</sup> Kangbao Zhong, <sup>‡,⊥</sup> Zhi-Keng Lin,<sup>¶</sup> Linbin Niu,<sup>†</sup> Zi-Qi Li,<sup>§</sup> Ruopeng Bai,\*,<sup>‡</sup> Keary M. Engle,\*,<sup>§</sup> and Yu Lan\*,<sup>†,‡</sup>

ABSTRACT: Reductive elimination is a key step in Ni-catalyzed cross-couplings. Compared with processes that proceed from Ni(III) or Ni(IV) intermediates,  $C(sp^3)$ – $C(sp^3)$  reductive eliminations from Ni(II) centers are challenging due to the weak oxidizing ability of Ni(II) species. In this report, we present computational evidence that supports a mechanism in which Zn coordination to the nickel center as a Z-type ligand accelerates reductive elimination. This Zn-assisted pathway is found to be lower in energy compared with direct reductive elimination from a σ-coordinated Ni(II) intermediate, providing new insight into the mechanism of Ni-catalyzed cross-coupling with organozine nucleophiles. Mayer bond orders, Hirshfield charge, Laplacians of the electron density, orbital and IRI analysis were conducted to elucidate details of the reductive elimination process and characterize the key intermediates. Theoretical calculations indicate a significant Z-type Ni–Zn interaction that reduces the electron density around the Ni center and accelerates reductive elimination. This mechanistic study of reductive elimination in Ni(0)-catalyzed conjunctive cross-couplings of aryl iodide, organozine regents, and alkenes is an important case study of the involvement of Zn-assisted reductive elimination in Ni catalysis. We anticipate that the novel Zn-assisted reductive elimination mode may extend to other cross-coupling process and explain the unique effectiveness of organozine nucleophiles in many instances.

## INTRODUCTION

Over the past few decades, nickel-catalyzed cross-coupling has become an integral tool in organic synthesis. <sup>1-3</sup> In addition to being a cheaper, earth-abundant alternative to precious metal catalysts, nickel exhibits several unique properties that lead to differentiated reactivity compared with other transition metals. <sup>4-6</sup> For example, Ni complexes can adopt both high- and low-spin configurations and are stable in a variety of oxidation states ranging from Ni(0) to Ni(IV). <sup>7-10</sup> These properties have been leveraged in the development of myriad Ni-catalyzed transformations to access products with diverse properties and functions.

In Ni-catalyzed cross-coupling reactions, reductive elimination forges the new covalent bond in the organic product and is thus a fundamental step in these processes. <sup>11-13</sup> In many Ni-catalyzed cross-couplings, the coupling partner compatibility is dictated by the rate and scope of the reductive elimination step. <sup>14-16</sup> Reductive elimination from Ni(III) or Ni(IV) species is typically facile. In contrast, owing to the weak oxidizing ability of Ni(II) species, Ni(II)/Ni(0) reductive elimination is typically more challenging (Scheme 1a). Hence, while Ni-catalyzed cross-couplings to form C(sp<sup>2</sup>)–C(sp<sup>3</sup>) and C(sp<sup>2</sup>)–X (X=O, N, halogens) bonds are typically accessible with appropriate ancillary ligands to accelerate the reductive elimination from Ni(II) species, <sup>17-19</sup> catalytic C(sp<sup>3</sup>)–C(sp<sup>3</sup>) cross-coupling via a Ni(0)/Ni(II) redox couple re-

mains challenge despite widespread interest during the past several years.  $^{20\cdot22}$ 

Recently, Ni-catalyzed conjunctive cross-couplings have attracted attention as powerful tools in organic synthesis (selected examples are shown in Scheme 1b). 1,23-29 In this type of reaction, the aryl halide electrophile, organometallic nucleophile, and  $\pi$ bond-containing substrate (often containing a proximal directing group) are merged together in a selective manner. Interestingly, when olefins are used as the  $\pi$ -bond component, this reaction can be used to construct a new C(sp<sup>3</sup>)-C(sp<sup>3</sup>) bond through a reductive elimination process. Organozinc reagents often serve as the nucleophile coupling partner in the absence of additional ligand, base or additives, with a low-valent Ni(0)/Ni(II) catalytic cycle commonly invoked. In these cases, the reductive elimination is often proposed to occur from Ni(II) intermediates. We thus wondered what mechanistic features of these catalytic processes allow C(sp<sup>3</sup>)-C(sp<sup>3</sup>) bond-formation formation to occur under such mild reaction conditions.

According to previous mechanistic studies of transition-metal-catalyzed cross-couplings, organozinc reagents have been proposed to serve various roles, including as the nucleophilic coupling partner, as a Lewis acid, or as a countercation. <sup>18,30,31</sup> Recently, organozinc reagents have been proposed to serve an additional role as Z-type ligands <sup>32,33</sup> for

<sup>†</sup> Green Catalysis Center, College of Chemistry, Zhengzhou University, Zhengzhou, Henan 450001, China

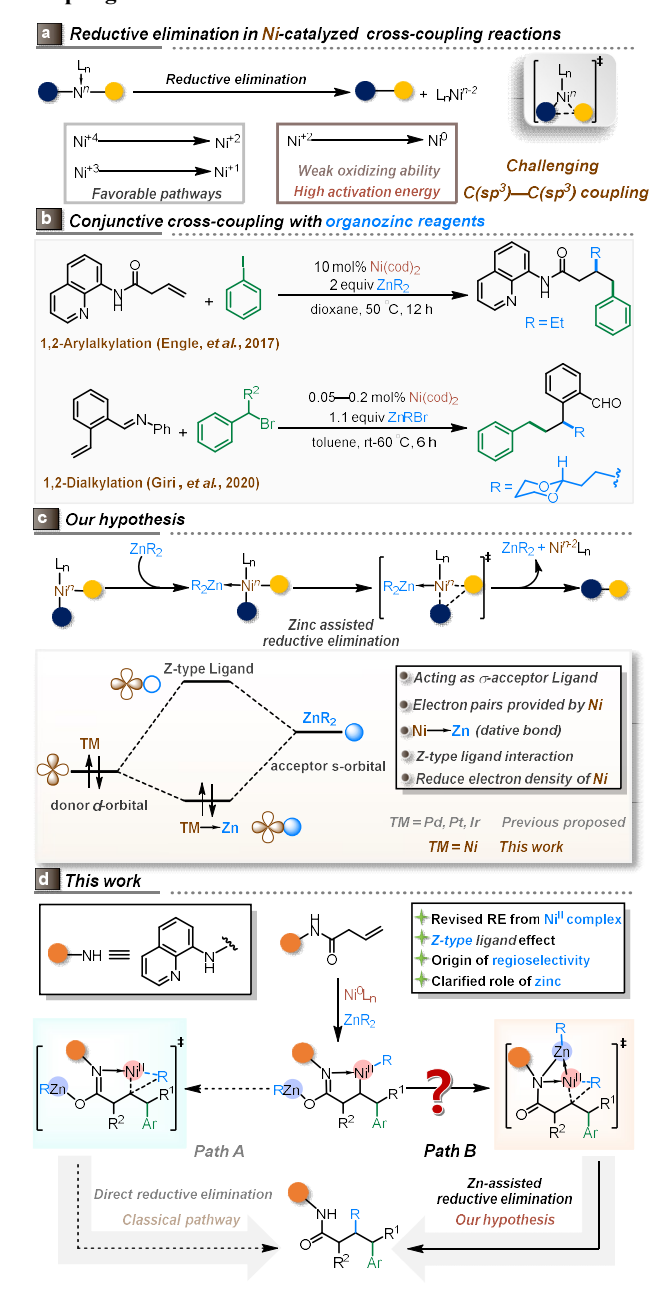
<sup>§</sup> Department of Chemistry, The Scripps Research Institute, 10550 N. Torrey Pines Rd., La Jolla, California 92037, USA

ZhengZhou JiShu Institute of AI Science, Zhengzhou, Henan 450000, China

<sup>&</sup>lt;sup>‡</sup> School of Chemistry and Chemical Engineering, Chongqing Key Laboratory of Theoretical and Computational Chemistry, Chongqing University, Chongqing 400030, China

<sup>¶</sup> Department of Chemistry, National University of Singapore 3 Science Drive 3, Singapore 117543, Republic of Singapore KEYWORDS: Reductive elimination, Z-type dative bond, Ni-catalysis, Zn-metaloligand, Cross-coupling.

Scheme 1. Reductive elimination in Ni-catalyzed crosscoupling reactions



late transition metals such as Rh, Ir, Pt, Pd, etc.34-38 We surmised that Ni would also be capable of engaging in Z-type dative bonding with Zn, which could give rise to distinct modes of reactivity in Ni-catalyzed cross-coupling reactions with organozinc reagents. In this case, the Zn atom acts as  $\sigma$ -acceptor ligand during dative bonding with Ni. A filled d-orbital of Ni provides an electron pair to an unfilled s-orbital of Zn (Scheme 1c). This is distinct from standard organic ligands such as phosphines and amines, which usually coordinate to transition metals mainly through  $\sigma$ -donation and in some cases through secondary  $\pi$ -back donation. Z-type coordination reduces the overall electron-density of the Ni atom, which we reasoned could be highly beneficial in facilitating C-C or C-X bond-forming reductive elimination processes from Ni centers. Experimental evidence for the proposed bonding interaction between Ni and Zn was recently reported the Martin group in a mechanistic investigation of a Ni-catalyzed C-O bond functionalization reaction, which included single-crystal characterization of a polymetallic Ni-Zn cluster.<sup>39</sup> A Ni-Zn complex was synthesized to uncovering the molecular interaction of Ni and Zn. With this idea in mind, we sought to apply computational techniques to explore the hypothesis that Zn-assisted reductive elimination is involved in the Ni-catalyzed conjunctive cross-coupling reactions (Scheme 1b).

While organozinc regents are commonly used as effective nucleophiles in Ni-catalyzed conjunctive cross-couplings, the lack of knowledge regarding the role of Zn in reductive elimination has hampered the full breadth of possibilities of Ni-catalyzed crosscoupling in organic synthesis. To better understand the details of the reductive elimination step, the present study focuses on the mechanism of Ni(0)-catalyzed conjunctive cross-coupling with aryl iodides and organozinc regents recently reported by the Engle group (Scheme 1d).23 Although the mechanism of Ni-catalyzed conjunctive cross-couplings has been investigated in several computational and experimental studies, 40-42 a detailed picture of the reductive elimination step in Ni(0)/Ni(II) catalytic processes, particularly in those lacking strongly coordinating ancillary ligands (e.g., phosphines), remains elusive. Therefore, we performed density functional theory (DFT) calculations to investigate the mechanism of reductive elimination in this type of reaction and clarify the role of Zn during the full catalytic cycle. In particular, we sought to elucidate whether the reaction proceeds by direct or Zn-assisted reductive elimination and what factors control the preferred reductive elimination mechanism in Ni(0)/Ni(II) redox cycles. Moreover, we wanted to verify the generality of Znassisted reductive elimination in Ni-catalyzed conjunctive crosscoupling reactions.

#### COMPUTATIONAL METHODS

All of the DFT calculations were performed with the Gaussian 09 series of programs.<sup>43</sup> The geometry optimization was conducted with the B3-LYP functional<sup>44,45</sup> and standard 6-31G(d) basis set (SDD basis set for Ni, Zn, and I atoms)<sup>46,47</sup>. Harmonic vibrational frequency calculations were performed for all stationary points to confirm whether they are local minima or transition state structures and to derive the thermochemical corrections for the enthalpies and free energies. The M06 functional<sup>48-50</sup> with the 6-311+G(d) basis set (Lan08+ basis set for Ni and Zn atoms, SDD basis set for I atom) was used to calculate the single-point energies and provide highly accurate energy information. 51-54 For the single-point energy calculations, solvent effects were taken into account by single-point calculations based on the gas-phase stationary points with the SMD<sup>55,56</sup> continuum solvation model. Unless otherwise noted, the experimental solvents used in this manuscript were dioxane. The values of  $\Delta G_{M06/solvent}$  in free energy profiles were obtained by Eq. 1, in which  $\Delta G_{\text{correction/gas}}$  is the thermochemical correction for the Gibbs free energy calculated B3-LYP/6-31G(d)/SDD level in the gas phase, and  $\Delta E_{\text{M06/solvent}}$  is M06/6the single point energy calculated at 311+G(d)/Lan08+/SDD level in solvent phase based on the gasphase stationary point.

# $\Delta G_{\text{M06/solvent}} = \Delta E_{\text{M06/solvent}} + \Delta G_{\text{correction/gas}} (1)$

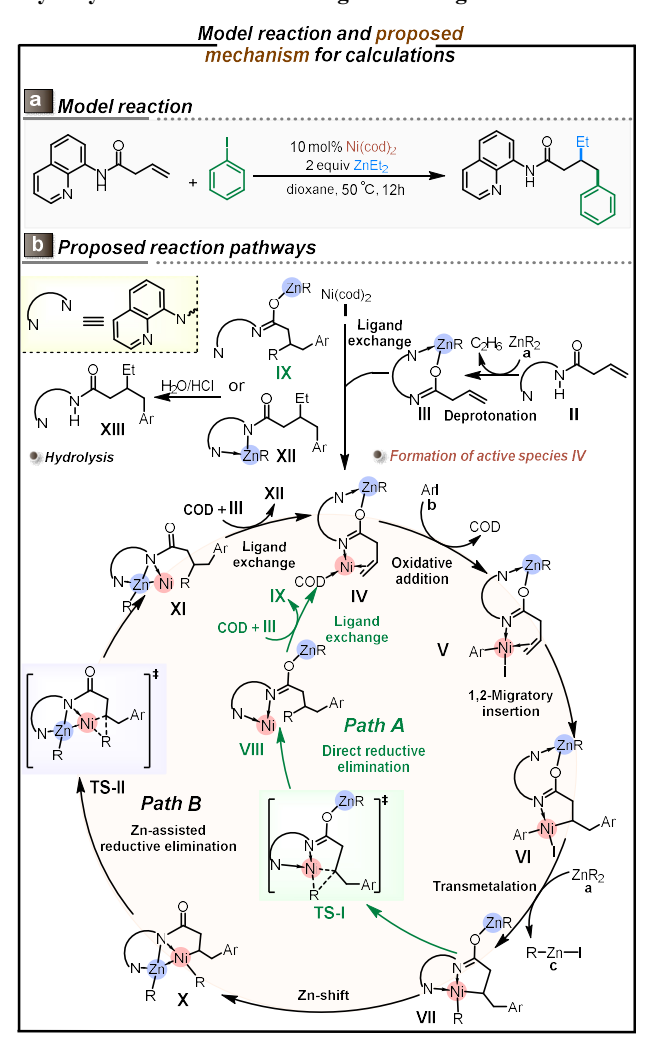
The three-dimensional molecular diagrams were generated with CYLView. The Mayer bond order, interaction region indicator (IRI) and Laplacian of the electron density were calculated at the B3-LYP/6-31G(d) level. Hirshfeld is a very popular atomic population method based on deformation density partition, and ADCH charge is the sum of original Hirshfeld charge and correction charge. ADCH atomic charges are reasonable in a chemical sense, molecular dipole moment is exactly reproduced, and the reproducibility of ESP is close to the atomic charges obtained from fitting ESP. The Laplacian of electron density is a function that is often investigated in the analysis of Atoms in Molecules (AIM). It represents the total curvature of the electron density; where it is posi-

tive, the electron density is divergent, and where it is negative, the electron density is aggregated. The Interaction Region Indicator (IRI) is used to show various types of interaction forces. IRI analysis can show both bond force and nonvalent bond force, and the resulting images provide clear visualizations.

#### RESULTS AND DISCUSSION

Mechanistic study of Ni(0)-catalyzed conjunctive cross-coupling with aryl iodides and organozinc regents. We first investigated the mechanism of Ni(0)-catalyzed conjunctive cross-coupling with aryl iodides and organozinc regents. A 1,2-arylalkylation reaction that employs the 8-aminoquinoline (AQ) directing group reported by the Engle group was chosen as the model reaction (Scheme 2a). As shown in Scheme 2b, deprotonation of reactant II with alkylzinc a generates organozinc intermediate III, which could coordinate with Ni(0) species I to provide catalytically active species IV. Oxidative addition of active species IV with aryl

Scheme 2. Potential reaction pathways for Ni(0)-catalyzed 1,2-arylalkylation of olefins with organozinc regents.



iodide **b** then gives Ni(II)-aryl intermediate **V**, which undergoes intramolecular 1,2-migratory insertion to form alkyl nickelacycle intermediate **VI** containing an iodide ligand. Subsequently, transmetalation of intermediate **VI** with alkylzinc **a** generates the key dialkylnickel intermediate **VII** with release of Zn salt **c**. Two possible pathways were then considered during our computational modeling of this reaction. In pathway A (green lines), direct reductive elimination from intermediate **VII** occurs via three-

membered ring transition state TS-I to give Ni(0) complex VIII with concomitant formation of the new C(sp<sup>3</sup>)-C(sp<sup>3</sup>) covalent bond. Then, this complex undergoes ligand exchange with 1,5cyclooctadiene (COD) and Zn-substrate adduct III to regenerate active species IV with release of Zn-hydroxy salt IX. Finally, the desired product XIII could be formed through hydrolysis of IX. Considering the high energy barrier anticipated for direct C(sp<sup>3</sup>)-C(sp<sup>3</sup>) reductive elimination from a Ni(II) center, another possible pathway B (black lines) involving initial Zn coordination as a Ztype ligand was also considered, which we reasoned may facilitate this challenging  $C(sp^3)$ – $C(sp^3)$  bond-forming step. In pathway B, a Zn-shift occurs before reductive elimination to form Z-type dative Ni-Zn intermediate X. Subsequently, Zn-assisted C(sp3)-C(sp<sup>3</sup>) reductive elimination from intermediate X proceeds via transition state TS-II to regenerate Ni(0) species XI, which then undergoes ligand exchange to regenerate active species IV with release of Zn-amino salt IX. The corresponding hydrolysis of IX also yields desired product XIII. DFT calculations were performed to investigate the mechanism for this Ni(0)-catalyzed coupling of aryl iodides and organozinc regents with alkenyl am-

Formation of active catalytic species and oxidative addition steps. The calculated free energy profile for formation of active catalytic species 7 is shown in Figure 1. Initially, coordination of reactant 1 to diethylzinc 2 gives intermediate 3, which is endergonic by 1.7 kcal/mol. The deprotonation step then occurs via sixmembered-ring transition state 4-ts to form amino-Zn intermediate 5. The activation free energy for this step from intermediate 1 is 19.6 kcal/mol, so it could easily occur at a reaction temperature of 50 °C. Subsequently, ligand exchange between intermediate 5 and Ni(COD)<sub>2</sub> 6 generates active Ni species 7 exergonically.

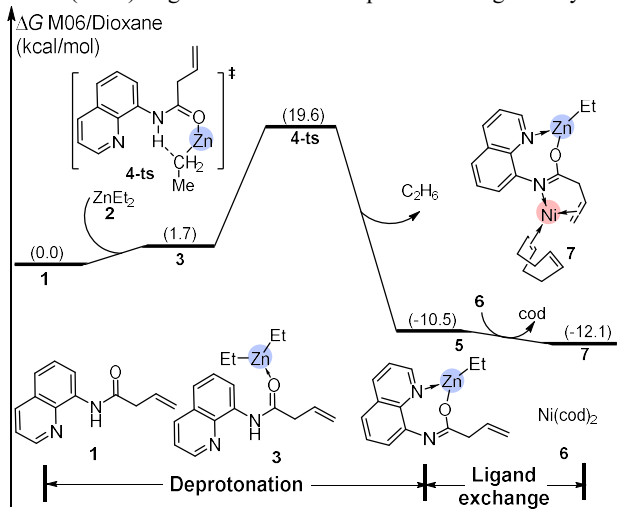


**Figure 1**. Free energy profile for the formation of active catalytic species 7 in Ni(0)-catalyzed conjunctive cross-coupling with aryl iodides and organozine regents. The energies are in kcal/mol and represent the relative free energies calculated at the M06/6-311+G(d) level in dioxane solvent.

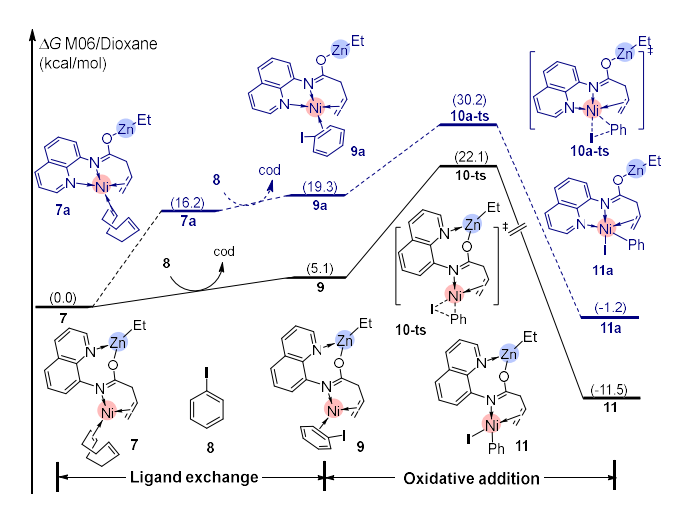


**Figure 2**. Free-energy profiles for the oxidative addition step in Ni(0)-catalyzed conjunctive cross-coupling with aryl iodides and organozine regents. The energies are in kcal/mol and represent the relative free energies calculated at the M06/6-311+G(d) level in dioxane solvent

Based on previous theoretical studies, oxidative addition of aryl iodide is usually invoked as the initial step in Ni(0)-catalyzed cross-coupling reactions. <sup>11,57</sup> As shown in Figure 2, the active species 7 was set as the relative zero point for the free energy profiles of the main catalytic cycle, where the N atom of quinoline group in AQ coordinates to Zn, and the N atom of the imine group coordinates to Ni. Considering the coordination mode of the AQ ligand, two possible oxidative addition pathways (black line and blue line in Figure 2) were taken into account in the calculations. In the black pathway, ligand exchange of 7 with iodobenzene 8

gives Ni(0) intermediate 9 with concomitant release of COD. This step is endergonic by 5.1 kcal/mol. Subsequently, oxidative addition occurs via three-membered-ring transition state 15-ts with an overall activation free energy of 22.1 kcal/mol to form Ni(II)(Ar)(I) 11. Notably the N,N-based AQ directing group coordinates to both the Zn and Ni centers with each of the two nitrogen atoms coordinating to one of the metals during the oxidative addition step in the black pathway.

On the other hand, AQ is an electron-donating ligand, which would be beneficial for oxidative addition of the Ni(0) species. Therefore, we investigated another possible pathway (blue lines in Figure 2) in which both N atoms from AQ coordinate to Ni. In this pathway, the isomerization from intermediate 7 to 7a is endergonic by 16.7 kcal/mol. One formed, intermediate 7a undergoes ligand exchange and oxidative addition to form Ni(II) intermediate 11a. Notably, the overall activation free energy of oxidative addition through the blue pathway is 30.2 kcal/mol, which is 8.1 kcal/mol higher than that through the black pathway. The energy barrier difference between these two pathways can be attributed to the coordination mode of AQ. In the black pathway, the N atom of the quinoline group in AQ stabilizes the Zn atom. Therefore, the black pathway is favorable for oxidative addition.

**1,2-Migratory insertion and transmetalation.** Figure 3a shows the calculated free energy profile for 1,2-migratory insertion and transmetalation. When intermediate **11** is formed, subsequent 1,2-migratory insertion could occur via transition state **12-ts** (solid line) or **14-ts** (dashed line) to give opposite regioisomers. The  $\gamma$ -arylated Ni(II)—alkyl intermediate **13** is formed via transition state **12-ts** with an activation free energy of 8.4 kcal/mol. Alternatively, the  $\beta$ -arylated Ni(II)—alkyl intermediate **15** is formed via insertion transition

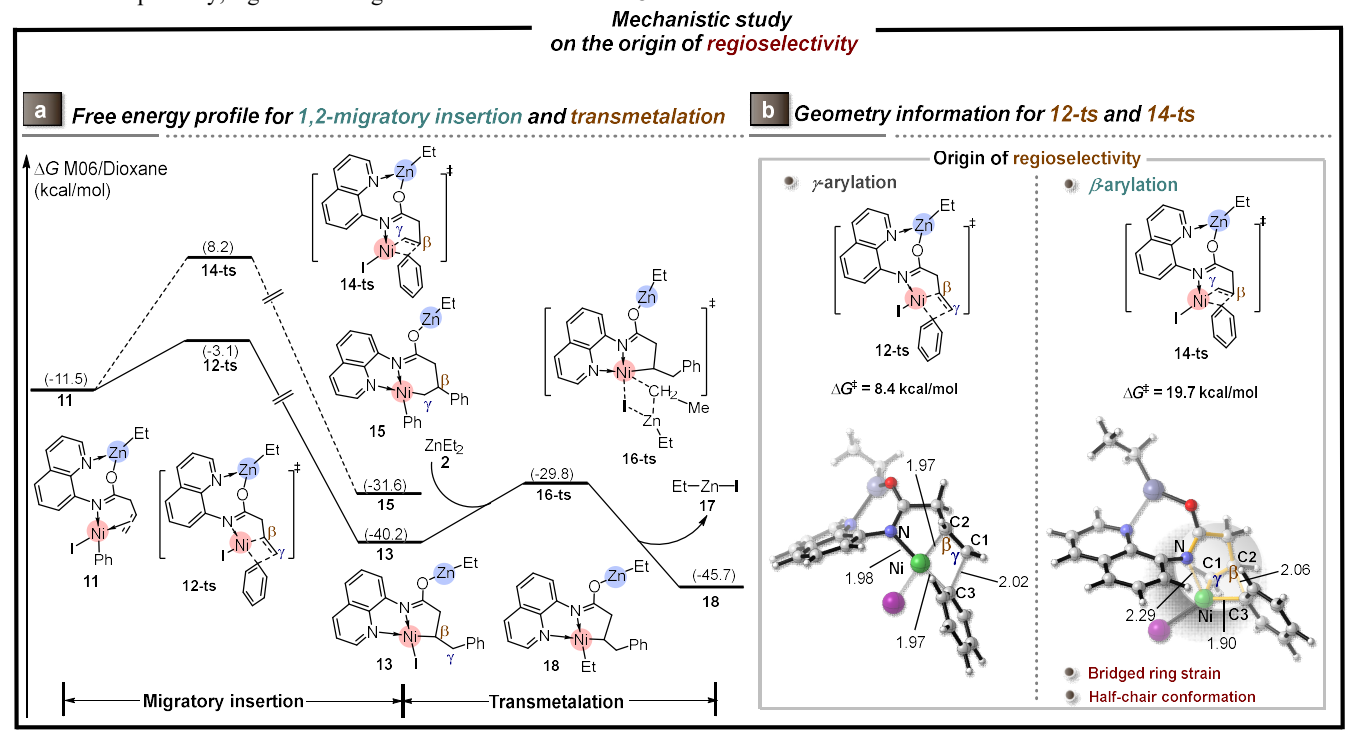


**Figure 3**. (a). Free-energy profiles for 1,2-migratory insertion and transmetalation in Ni(0)-catalyzed conjunctive cross-coupling with aryliodides and organozinc reagents. The energies are in kcal/mol and represent the relative free energies calculated at the M06/6-311+G(d) level in dioxane solvent. (b). Optimized geometries of transition states **12-ts** and **14-ts**. The bond lengths are in angstroms.

state **14-ts** with an activation free energy of 19.7 kcal/mol, which is 11.3 kcal/mol higher than that of  $\gamma$ -arylation. Furthermore, the

relative free energy of intermediate 13 is 8.6 kcal/mol lower than that of intermediate 15. In consideration of both kinetic and thermodynamic effects,  $\gamma$ -arylation is the major pathway for 1,2-olefin

migratory insertion. When intermediate 13 is formed, a rapid transmetalation could occur in presence of excess diethylzine 2 to

give a more stable Ni(II)-alkyl complex 18 with an activation free energy of only 10.4 kcal/mol.

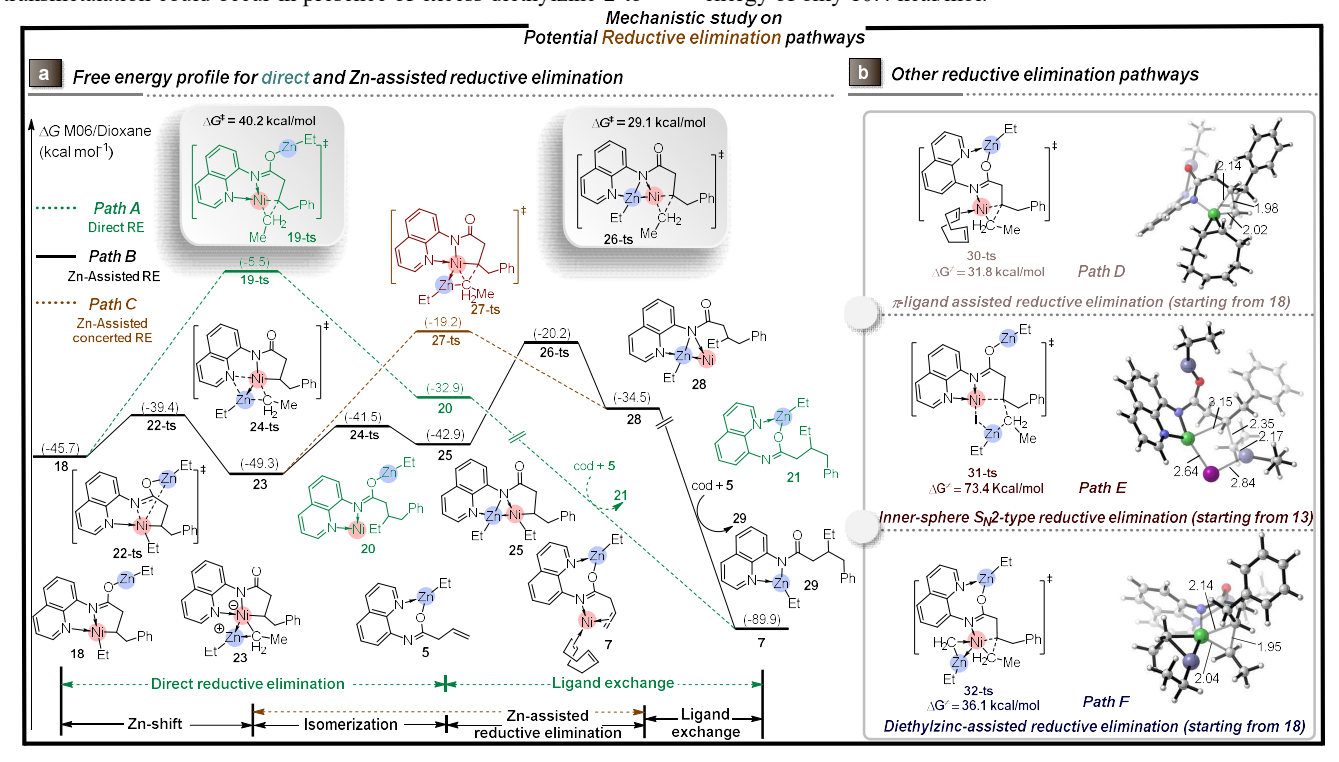


**Figure 4**. a. Free-energy profiles for direct and Zn-assisted reductive elimination steps in Ni(0)-catalyzed conjunctive cross-coupling with aryl iodides and organozinc regents. b. Transition states and optimized geometries for other possible reductive elimination pathways (see supporting information for details). The energies are in kcal/mol and represent the relative free energies calculated at the M06/6-311+G(d) level in dioxane solvent. The bond lengths are in angstroms.

Reductive elimination. Next, we calculated the free energy profiles for possible reaction pathways for the reductive elimination step. According to previous theoretical and experimental studies, direct reductive elimination is usually considered to occur in Ni(0)-catalyzed cross-coupling reactions for the formation of  $C(sp^2)$ – $C(sp^2)$  or  $C(sp^2)$ -X (X = O, N, S) bonds. Thus, we initially calculated the free energy profile for direct reductive elimination pathway A (green lines in Figure 4a). In this pathway, reductive elimination from Ni(II) intermediate 18 proceeds via a threemembered-ring transition state 19-ts to give Ni(0)-imine intermediate 20. Surprisingly, the calculated activation free energy for the reductive elimination of two sp<sup>3</sup> carbogenic groups is up to 40.2 kcal/mol, which indicates that the direct reductive elimination is difficult to achieve under the reported reaction conditions (50 °C, 12 h). Assuming that intermediate 20 is indeed generated through this step, 20 would subsequently undergo ligand exchange with free COD and Zn-bound alkene substrate (intermediate 5) to regenerate catalytic species 7 with concomitant release the product as its Zn salt (intermediate 21). Finally, the desired product is formed by hydrolysis during work-up. Due to the high activation free energy of direct reductive elimination, pathway A can be excluded. Previous studies indicated that Zn complexes can serve as Z-type ligands for coordination to Pd, Pt, Ru and Ir. Martin's work has provided evidence for a Ni-Zn interaction during Nicatalyzed C-O cross-coupling.<sup>39</sup> It is noteworthy that the Z-type ligand often acts as  $\sigma$ -acceptor, which is distinct from the  $\sigma$ -

donative AQ ligand. Therefore, we hypothesized that Zn may promote reductive elimination when it coordinates to Ni through dative bonding as a Z-type ligand. Following this idea, an intramolecular Zn-shift could occur via transition state 22-ts resulting in the formation of a Ni-Zn Z-type dative bond in intermediate 23. The energy barrier for this step is only 6.3 kcal/mol. Two possible reductive elimination pathways, B and C (brown and black lines, respectively, in Figure 4a), were considered for the following steps. In Zn-assisted reductive elimination pathway B, we found that the Z-type, datively bound organozine ligand in intermediate 23 can insert into Ni-N bond via isomerization transition state 24ts with a free energy barrier of 7.8 kcal/mol. The generation of intermediate 25 with a N-Ni-Zn three-membered-ring is endergonic by 6.4 kcal/mol. Zn-assisted C(sp<sup>3</sup>)-C(sp<sup>3</sup>) reductive elimination then occurs via transition state 26-ts to form Zn-Ni(0) intermediate 28. The overall activation free energy for Zn-assisted reductive elimination in path **B** is 29.1 kcal/mol, which is 11.1 kcal/mol lower than that of the reductive elimination in path A. Alternatively, in concerted Zn-Assisted reductive elimination path C, the calculated activation free energy for this type Zn-assisted reductive elimination via transition state 27-ts is 30.1 kcal/mol, which is 1.1 kcal/mol higher than that of path B. The generated unstable intermediate 28 could undergo ligand exchange with COD and preorganized intermediate 5 to regenerate active species 7 with concomitant release of the product, as its Zn-amino salt 29. Finally, the desired product can be achieved by

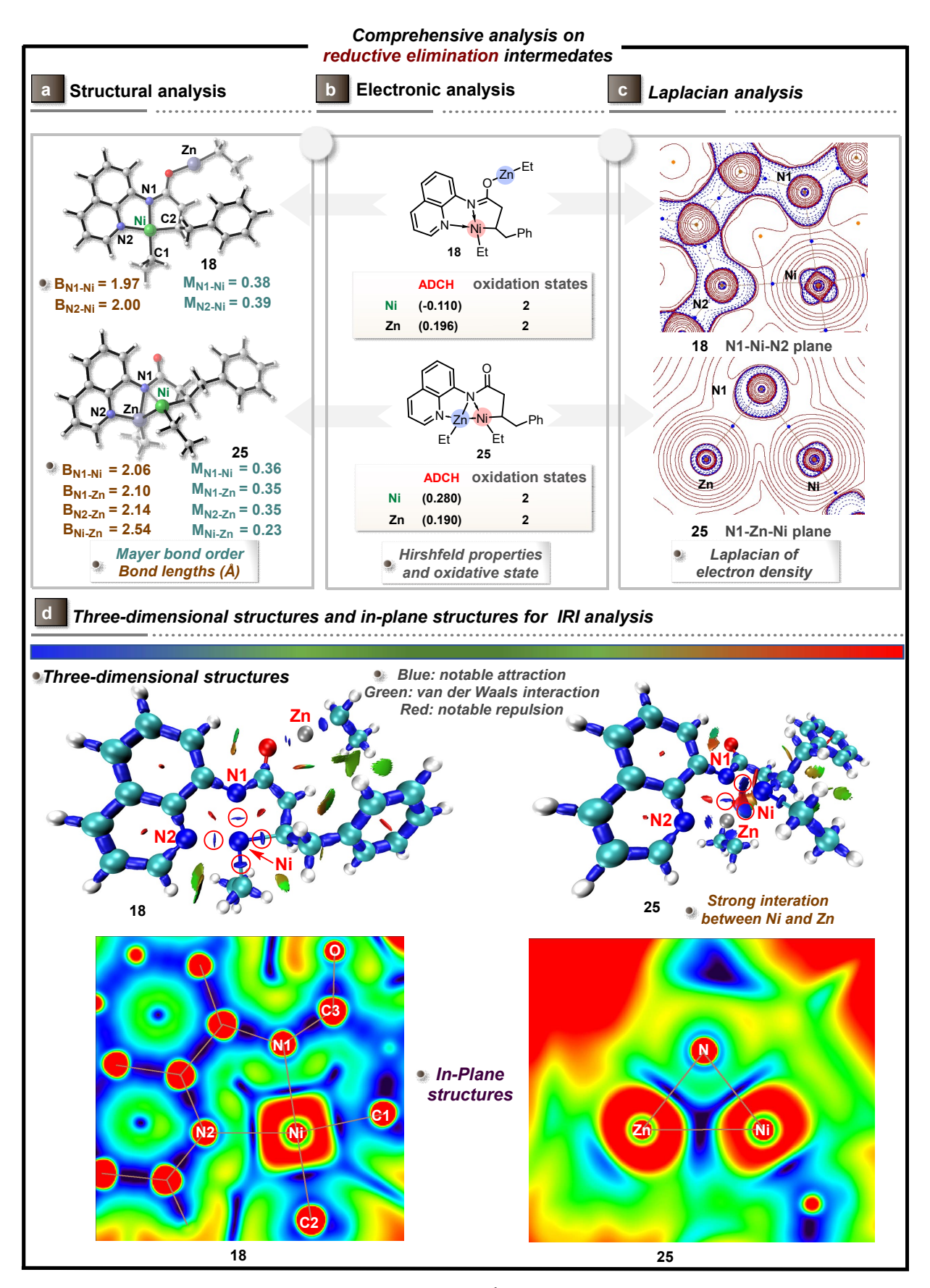


Figure 5. (a). Optimized geometry information, including bond lengths (Å) and Mayer bond orders for intermediate 18 and 25; (b). Calculated Hirshfeld charge analysis; (c). Laplacian of electron density of Intermediate 18 and 25; (d). Three-dimensional structures and in-plane structures for IRI analysis of intermediates 18 and 25.

hydrolysis during work-up. Furthermore, we have also calculated other potential reductive elimination pathways (Figure 4b and Figure S2, see supporting information for details), including  $\pi$ ligand assisted reductive elimination (path **D**), inner-sphere nucleophilic substitution-typereductive elimination (path E) and diethylzinc-assisted reductive elimination (path F). Moreover, the Ni-I-Zn assisted reductive elimination are also considered (Figure S8, see supporting information for details). The calculated activation free energies for those possibilities, however, are higher than that of Zn-assisted reductive elimination via transition state 26-ts. The computational results are consistent with Zn-assisted reductive elimination path **B** as the most favorable pathway and further indicate that reductive elimination is the turnover-limiting step of the overall catalytic cycle. Moreover, other organozinc reagents, such as EtZnI, were also considered in reductive elimination (Figure S10, see supporting information for details). The calculated result demonstrate the competence of alkylzinc halide salts in the conjunctive cross-coupling, consistent with the published experimental results.

According to the computational results above, a reasonable reaction pathway for Ni(0)-catalyzed conjunctive cross-coupling with aryl iodides and organozinc regents can be proposed. The coordination and deprotonation of reacting alkene 1 with diethylzinc 2 followed by ligand exchange with Ni(cod)<sub>2</sub> 6 generates Ni(0)-imine intermediate 7, which is the active species in the catalytic cycle. Oxidative addition with iodobenzene 8 generates Ni(II) iodide intermediate 11, which undergoes intramolecular olefin insertion to give  $\gamma$ -arylated intermediate 13. The followed

transmetalation with excess diethylzinc 2 then forms Ni(II)-alkyl intermediate 18, which undergoes a Zn-shift to afford intermediate 23 containing a Z-type Ni-Zn dative bond. Zn inserts into the Ni-N bond, which results in another Z-type complex 25 with a N-Ni-Zn three-membered-ring. In this intermediate, the Zn and Ni atoms are co-localized by coordination to the two nitrogen atoms of AQ, leading to a spatially and conformationally restricted coordination environment. Then a newly proposed Zn-assisted reductive elimination forms the new C(sp<sup>3</sup>)-C(sp<sup>3</sup>) bond, which may be important to consider in other Ni-catalyzed cross-coupling reactions involving organozinc reagents. Active catalyst 7, can be regenerated by ligand exchange with release of Zn salt of the product, intermediate 29, which can be further transformed to protonated form of the product by hydrolysis. Zn-assisted reductive C(sp<sup>3</sup>)-C(sp<sup>3</sup>) elimination is determined to be the ratedetermining step of the whole catalytic cycle. The computational results demonstrate that organozinc regent is not only used as Brønsted base and transmetalation regent, but also can be regarded as a Z-type ligand that accelerates reductive elimination. These results explain why C(sp<sup>3</sup>)-C(sp<sup>3</sup>) bond formation can be efficiently achieved in this type reaction under such mild reaction conditions.

Comprehensive analysis of Zn-assisted reductive elimination Based on the mechanistic studies, we wondered what factors are important to Zn-assisted  $C(sp^3)$ – $C(sp^3)$  reductive elimination in Ni(0)-catalyzed conjunctive cross-coupling. Moreover, we also sought to clarify how the Z-type metalloligand accelerates the reductive elimination step in this type of reaction.

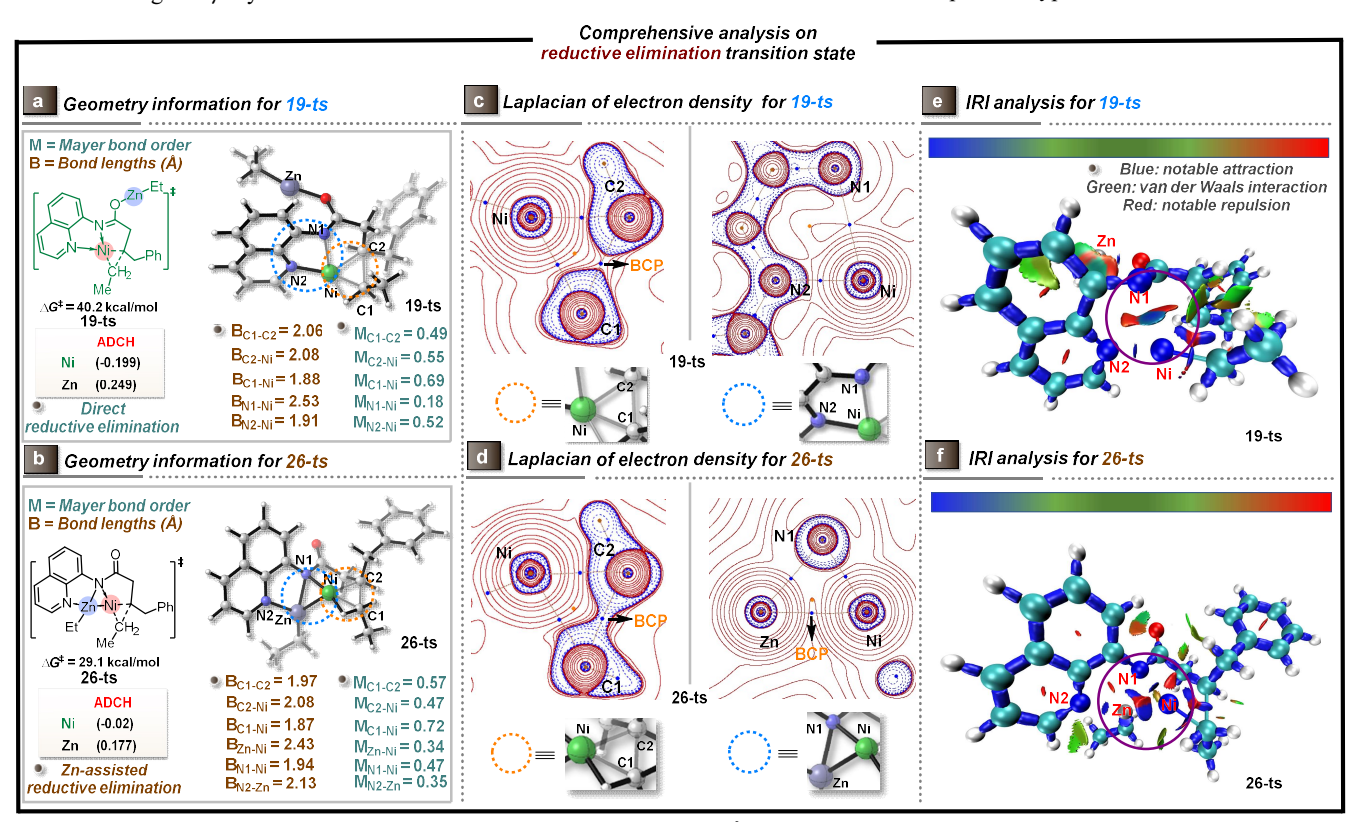


Figure 6. (a). Optimized geometry information, including bond lengths (Å), Hirshfeld charge and Mayer bond orders for transition state 19-ts; (b). Optimized geometry information, Hirshfeld charge and Mayer bond orders for transition state 26-ts; (c). Laplacian of electron density of transition state 19-ts; (d). Laplacian of electron density for transition state 26-ts, values of Laplacian of electron densities ( $\nabla^2_{\rho}$ ) in  $10^{-1}$  atomic units; (e). Three-dimensional structures for IRI analysis of transition state 26-ts.

To shed light on these interrelated issues, initially we performed a comprehensive analysis that included consideration of the structural (Figure 5a) and electronic properties (Figure 5b), the

Laplacian of electron density (Figure 5c) and IRI analysis (Figure 5d) of pre-reductive elimination intermediates **18** and **25**. As shown in Figure 4a, the calculated Mayer bond orders of Ni–N1 and Ni–N2 in intermediate **18** are 0.38 and 0.39, with bond

lengths of 1.97 and 2.00 Å, respectively. In contrast, the calculated Mayer bond orders of Ni-N1, Ni-Zn, Zn-N1 and Zn-N2 in intermediate 25 are 0.36, 0.23, 0.35 and 0.35, respectively. The bond lengths of Ni-N1, Ni-Zn, Zn-N1, and Zn-N2 in this intermediate are 2.06, 2.54, 2.10, and 2.14 Å, respectively. These results reveal that the AQ ligand coordinates to Zn directly in complex 25. Meanwhile, Z-type coordination of the Znmetalloligand to Ni results in an observable interaction between Ni and Zn. The electronic analysis (Figure 5b) reveals that the electron density on the Ni atom is significantly decreased by the Z-type coordination of Zn in complex 25, while the electron density on the Zn atom is slightly changed. This result shows that the Zn-metalloligand is accessible to decrease the electron density on Ni atom in reacting center, which would promote the reductive elimination to yield a Ni(0) species. Moreover, both of the calculated oxidation states for Ni and Zn in intermediate 25 are +2, which further indicates a coordination interaction between Zn and Ni without an associated redox event. The Laplacians of electron density in the planes defined by N1, N2, and Ni of intermediate 18 and by N1, Zn, and Ni of intermediate 25 were plotted using AIM theory (Figure 5c). In 18, the bond critical point (BCP) was identified in the N1-Ni and N2-Ni bonds. Alternatively, in 25, two BCPs were detected between the N1-Zn and N2-Zn bonds, whereas no BCP was identified in the Ni-Zn bond. These results reveal a series of weak interactions in 25. The IRI analysis (Figure 5d) also indicated that the Ni-N1 and Ni-N2 interactions in 18 were strongly attractive (dark blue area), analogous to coordination interactions. Meanwhile, the Ni-N1 and Zn-Ni interactions were strongly attractive (dark blue area) in intermediate 25, which indicates bonding interaction of Zn-Ni. All of these analyses strongly support a Z-type coordination of Zn to Ni, which leads to a decrease in the electron density of the reacting Ni center.

To further understand the differences between direct and Zn-assisted reductive elimination, we then compared the geometries, electronic parameters, Mayer bond orders, Laplacians of electron density. and IRI analyses of the two key reductive elimination transition states. 19-ts and 27-ts. As shown in Figure 6a, in the geometry of transition state 19-ts the bond lengths of the N1–Ni and N2–Ni are 2.53 and 1.91 Å, respectively. In contrast, those bond lengths in intermediate 18 (Figure 5a) are 1.97 and 2.00 Å, respectively. These results indicate that  $\sigma$ -donation from N1 of the directing group AQ is partially weakened during the direct reductive elimination, leading to a higher energy barrier for this step.

On the other hand, in Figure 6b, the lengths of the N1–Ni, N2–Zn, and Ni–Zn bonds in transition state **26-ts** are 1.94, 2.13 and 2.43 Å, respectively. In contrast, those bond lengths in intermediate **26** (Figure 5a) are 2.06, 2.10, and 2.54 Å, respectively. The bond lengths of the N1–Ni and Ni–Zn bonds in **26-ts** are significantly reduced. Meanwhile, the calculated Mayer bond orders of the N1–Ni and Ni–Zn bonds in **26-ts** are 0.47 and 0.35, which are obviously higher than those of **25**. The calculated results indicate that the Z-type metalloligand dative bond with Ni is strengthened during reductive elimination, which is distinct from the σ-donating ligand AQ. The stronger Ni–Zn bond in transition state **26-ts** indicates that this dative interaction stabilizes this transition state, which results in a lower activation free energy.

In both cases, with and without the involvement of Z-type Zn-metalloligand, the electronic analysis reveals that the electron density on the Ni atom is significantly increased when reductive elimination takes place due to the electron transfer that is associated with formal reduction of Ni. The effect of the Zn ligand on electron density is substantial, as the Hirshfeld charge value of Ni is 0.280 in intermediate 25 in the presence of Z-type Zn-metalloligand, compared with -0.110 in 18 without Z-type dative Zn. These results indicate that the Z-type Zn-metalloligand is

beneficial for promoting the electron transfer from alkyl moiety to Ni atom resulting in acceleration of reductive elimination. The Laplacians of the electron density in the planes defined by C1, C2, and Ni of transition states 19-ts and 26-ts are shown in Figures 6c and 6d. The electron density around C1 is significantly polarized toward the C2 center in transition state 26-ts compared with that in transition state 19-ts. This difference indicates that there is a stronger mutual attraction between C1 and C2 in 26-ts than that in 19-ts. Furthermore, in 26-ts, the BCP was detected between the Ni–Zn bond with a  $\nabla^2 \rho$  value of 0.54, which stands in contrast to intermediate 25 in which no BCP was identified in Ni-Zn bond (Figure 5c). This also reveals a strengthened Ni-Zn interaction in 26-ts that promotes reductive elimination. The IRI analysis (Figure 6e) also reveals that the Ni-N1 interaction in transition state 19-ts is weakly attractive (pale blue area). Meanwhile, the Ni-Zn interaction is strongly attractive (dark blue area in Figure 6f) in transition state 26-ts, which can be confirmed by the Laplacians of the electron density in transition states 19-ts and **26-ts**. It also supports the notion that the N1–Ni coordination bond is gradually weaken during direct reductive elimination, while the Ni-Zn bond remains strong during this step. Therefore, the electron density of nickel is dispersed by zinc, resulting in facile reductive elimination in transition state 26-ts.

According to the abovementioned analysis on intermediates 18 and 25 and transition states 19-ts and 26-ts in both direct and Zn-assisted reductive elimination, an observable Ni–Zn interaction is determined to exist in the Zn-assisted reductive elimination step. Unlike the  $\sigma$ -donative coordination of AQ, the Z-type dative bonding between Zn and Ni diminishes the electron density on Ni atom, which promotes reductive elimination. It is noteworthy that the  $\sigma$ -donating ligand AQ partially dissociates during direct reductive elimination. In contrast, the Z-type Zn-metalloligand dative bonding with Ni strengthens during reductive elimination in the Zn-assisted pathway that accelerates this step.

Verifying the Zn-assisted reductive elimination in Ni(0)catalyzed conjunctive cross-coupling with alkyl iodide and organozinc regents. The above theoretical investigation has led to a revised mechanism for C(sp<sup>3</sup>)-C(sp<sup>3</sup>) reductive elimination of Ni(II) species facilitated Z-type dative Zn coordination. To test the generality of this model in Ni(0)-catalyzed cross-coupling, we carried out a mechanistic study of reductive elimination in another Ni(0)-catalyzed conjunctive cross-coupling with alkyl iodides and organozinc reagents, which was recently reported by the Giri group.<sup>25</sup> As shown in Figure 7a, (dioxanylethyl)zinc bromide is used as nucleophile for the construction of a new  $C(sp^3)$ – $C(sp^3)$ bond in the absence of ligand, base, oxidant, or other additives. In Figure 7b, both of the direct reductive elimination (Path A, green pathway) and the revised Zn-assisted assisted reductive elimination (Path B, black pathway) were considered in this work. When Ni(II)-dialkyl intermediate 33 is formed, Zn(II) species can coordinate through a Z-type dative bond resulting in complex 37, which is exergonic by 2.3 kcal/mol. Interestingly, the overall activation free energy of direct reductive elimination is up to 24.3 kcal/mol via transition state 34-ts even using  $\pi$ -accepted alkene ligand COD, which is invoked to be beneficial for reductive elimination in previous theoretical studies.<sup>58</sup> Alternatively, the activation free energy of Zn-assisted reductive elimination via transition state 38-ts dips to 15.9 kcal/mol, which is 8.4 kcal/mol lower than that of the direct process via transition state 34-ts. Geometric information of intermediate 37 and transition state 38-ts are given in Figure 7c. The Ni-Zn bond lengths of 37 and 38-ts are 2.58 and 2.63 Å, respectively, which also indicates a Ni–Zn interaction that assists reductive elimination. Therefore, Zn-assisted reductive elimination is more favorable than direct reductive elimination in this second case study involving Ni(0)-catalyzed conjunctive cross-coupling with alkyl iodides and organozinc reagents. This result further supports our hypothesis that organozine reagents can play a more complex role than previously appreciated as Z-type ligands that accelerate reductive elimination in Ni(0)-catalyzed cross-coupling reactions.

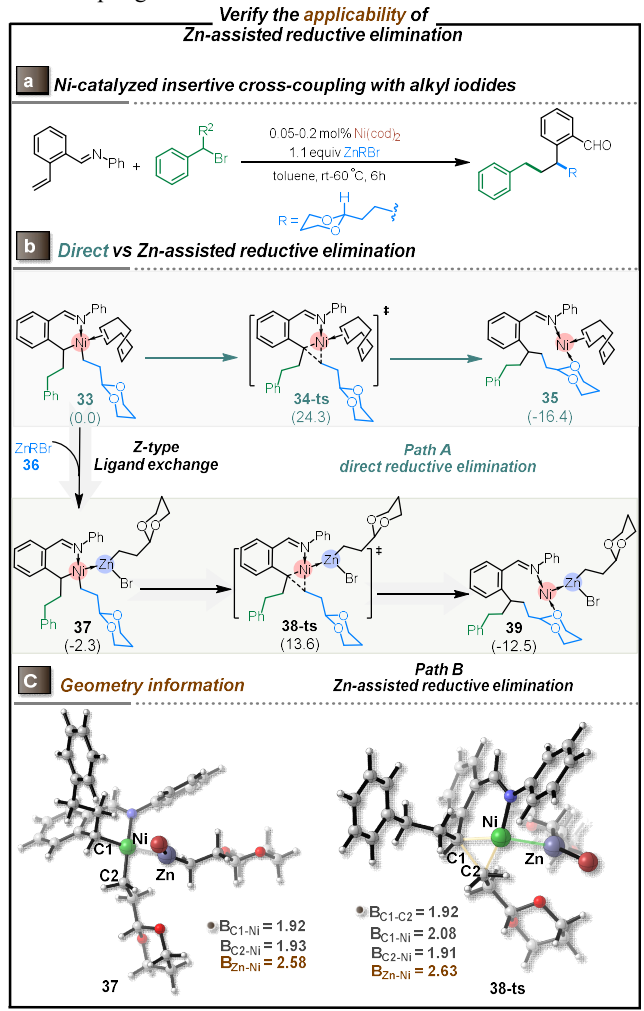


**Figure 7.** (a). Model reaction; (b). Calculations for direct and Zn-assisted reductive elimination in Ni(0)-catalyzed conjunctive cross-coupling with alkyl iodides and organozinc reagents. The energies are in kcal/mol and represent the relative free energies calculated at the M06/6-311+G(d) level in toluene solvent. (c). Optimized geometries of **37** and **38-ts**. The bond lengths are in angstroms.

# CONCLUSIONS

In this work, a revised mechanism for reductive elimination in Ni(0)-catalyzed conjunctive cross-couplings with organohalides and organozinc reagents is proposed, in which Zn plays a previously unappreciated role as a Z-type ligand. Distinct from typically invoked a direct reductive elimination mechaniss, the dialkylnickel(II) intermediate that precedes reductive elimination undergoes an intramolecular Zn-shift and insertion to give a Ztype Ni-Zn complex, from which Zn-assisted reductive elimination forms the new C(sp<sup>3</sup>)-C(sp<sup>3</sup>) bond. Zn-assisted reductive elimination was determined to be the turnover-limiting step in this reaction, and the calculated overall activation free energy is much lower than that of the direct reductive elimination. The Mayer bond orders, Laplacians of electron density and IRI analysis revealed an observable Ni-Zn interaction during Zn-assisted reductive elimination; Hirshfield charge analysis revealed that the Ztype dative bond between Zn and Ni significantly reduces the electron density on Ni atom which promotes reductive elimination. These findings proved to be general across two different Ni(0)-catalyzed conjunctive cross-couplings with both aryl and benzyl coupling partners involving different families of alkene substrates with distinct directing groups. The calculated results presented herein contribute to a better understanding of the role for organozinc regents in Ni-mediated  $C(sp^3)$ – $C(sp^3)$  bond formation beyond previously appreciated roles as Brønsted base, transmetalation partner, or Lewis acid. Future efforts will focus on gathering additional experimental evidence to probe the involvement of Ni–Zn bonding in various catalytic reactions and exploiting these interactions in novel reaction design. We anticipate that this theoretical framework will be practically valuable in guiding further experimental investigations.

#### ASSOCIATED CONTENT

# **Supporting Information**

This material is available free of charge via the Internet at <a href="http://pubs.acs.org">http://pubs.acs.org</a>.

Additional computational details and Cartesian coordinates (PDF)

## **AUTHOR INFORMATION**

## **Corresponding Author**

Ruopeng Bai – School of Chemistry and Chemical Engineering, Chongqing Key Laboratory of Theoretical and Computational Chemistry, Chongqing University, Chongqing 400030, China; orcid.org/0000-0002-1097-8526; Email: ruopeng@cqu.edu. cn. Keary M. Engle – Department of Chemistry, The Scripps Research Institute, 10550 N. Torrey Pines Rd., La Jolla, California 92037, USA; orcid.org/0000-0003-2767-6556; Email: keary @scripps.edu.

Yu Lan – Green Catalysis Center, College of Chemistry, Zhengzhou University, Zhengzhou, Henan, P. R. China 450001; School of Chemistry and Chemical Engineering, Chongqing Key Laboratory of Theoretical and Computational Chemistry, Chongqing University, Chongqing 400030, China; orcid.org/0000-0002-2328-0020; Email: lanyu@cqu.edu.cn.

#### Authors

**Tao Zhang** – Green Catalysis Center, College of Chemistry, Zhengzhou University, Zhengzhou, Henan, P. R. China 450001; ZhengZhou JiShu Institute of AI Science, Zhengzhou, Henan, China 450000.

Kangbao Zhong – School of Chemistry and Chemical Engineering, Chongqing Key Laboratory of Theoretical and Computational Chemistry, Chongqing University, Chongqing 400030, China. **Zhi-Keng Lin** – Department of Chemistry, National University of Singapore 3 Science Drive 3, Singapore 117543

Linbin Niu – Green Catalysis Center, College of Chemistry, Zhengzhou University, Zhengzhou, Henan, P. R. China 450001 Zi-Qi Li – Department of Chemistry, The Scripps Research Institute, 10550 N. Torrey Pines Rd., La Jolla, California 92037, USA

# Notes

 $^{\perp}$  Tao Zhang and Kangbao Zhong contributed equally to the manuscript

The authors declare no competing financial interests.

## ACKNOWLEDGMENT

This work was supported by the National Natural Science Foundation of China (NO. 21772020, 21822303, 22003006, 22101265),

and the Ministry of Science and Technology of the People's Republic of China, and the United States National Science Foundation (CHE-2102550). Bristol Myers Squibb is acknowledged for Graduate Fellowship (Z.-Q.L.).

## REFERENCES

- (1) Wickham, L. M.; Giri, R. Transition Metal (Ni, Cu, Pd)-Catalyzed Alkene Dicarbofunctionalization Reactions. *Acc. Chem. Res.* **2021**, *54*, 3415–3437.
- (2) Xue, W.; Jia, X.; Wang, X.; Tao, X.; Yin, Z.; Gong, H. Nickel-Catalyzed Formation of Quaternary Carbon Centers Using Tertiary Alkyl Electrophiles. *Chem. Soc. Rev.* **2021**, *50*, 4162–4184.
- (3) Zhu, C.; Yue, H.; Jia, J.; Rueping, M. Nickel-Catalyzed C-Heteroatom Cross-Coupling Reactions under Mild Conditions via Facilitated Reductive Elimination. *Angew. Chem. Int. Ed.* **2021**, *60*, 17810–17831.
- (4) Diccianni, J. B.; Diao, T. Mechanisms of Nickel-Catalyzed Cross-Coupling Reactions. *Trends. Chem* **2019**, *1*, 830–844.
- (5) Jana, R.; Pathak, T. P.; Sigman, M. S. Advances in Transition Metal (Pd, Ni, Fe)-Catalyzed Cross-Coupling Reactions Using Alkyl-Organometallics as Reaction Partners. *Chem. Rev.* **2011**, *111*, 1417-1492.
- (6) Tasker, S. Z.; Standley, E. A.; Jamison, T. F. Recent Advances in Homogeneous Nickel Catalysis. *Nature* **2014**, *509*, 299-309.
- (7) Camasso, N. M.; Sanford, M. S. Design, Synthesis, and Carbon-Heteroatom Coupling Reactions of Organometallic Nickel(IV) Complexes. *Science* **2015**, *347*, 1218-1220.
- (8) Lin, C. Y.; Power, P. P. Complexes of Ni(i): A "Rare" Oxidation State of Growing Importance. *Chem. Soc. Rev.* **2017**, *46*, 5347-5399.
- (9) Sperger, T.; Sanhueza, I. A.; Kalvet, I.; Schoenebeck, F. Computational Studies of Synthetically Relevant Homogeneous Organometallic Catalysis Involving Ni, Pd, Ir, and Rh: An Overview of Commonly Employed DFT Methods and Mechanistic Insights. *Chem. Rev.* **2015**, *115*, 9532-9586.
- (10) Zheng, B.; Tang, F.; Luo, J.; Schultz, J. W.; Rath, N. P.; Mirica, L. M. Organometallic Nickel(III) Complexes Relevant to Cross-Coupling and Carbon-Heteroatom Bond Formation Reactions. *J. Am. Chem. Soc.* **2014**, *136*, 6499-6504.
- (11) Diccianni, J.; Lin, Q.; Diao, T. Mechanisms of Nickel-Catalyzed Coupling Reactions and Applications in Alkene Functionalization. *Acc. Chem. Res.* **2020**, *53*, 906-919.
- (12) Jiang, T.; Zhang, H.; Ding, Y.; Zou, S.; Chang, R.; Huang, H. Transition-Metal-Catalyzed Reactions Involving Reductive Elimination Between Dative Ligands and Covalent Ligands. *Chem. Soc. Rev.* **2020**, *49*, 1487-1516.
- (13) Lan, Y. Computational Methods in Organometallic Catalysis: From Elementary Reaction to Mechanism. WILEY-VCH GmbH: Weinheim, Germany, **2021**; Chapter 5.
- (14) Jin, L.; Zhang, H.; Li, P.; Sowa, J. R., Jr.; Lei, A. What is the Rate of the Csp2-Csp2 Reductive Elimination Step? Revealing An Unusually Fast Ni-Catalyzed Negishi-Type Oxidative Coupling Reaction. *J. Am. Chem. Soc.* **2009**, *131*, 9892-9893.
- (15) Lohrey, T. D.; Cusumano, A. Q.; Goddard, W. A., 3rd; Stoltz, B. M. Identifying the Imperative Role of Metal-Olefin Interactions in Catalytic C-O Reductive Elimination from Nickel(II). *ACS Catal* **2021**, *11*, 10208-10222.

- (16) Simon, C. M.; Dudra, S. L.; McGuire, R. T.; Ferguson, M. J.; Johnson, E. R.; Stradiotto, M. Identification of a Nitrenoid Reductive Elimination Pathway in Nickel-Catalyzed C–N Cross-Coupling. *ACS Catal.* **2022**, *12*, 1475-1480.
- (17) Hazari, N.; Melvin, P. R.; Beromi, M. M. Well-defined Nickel and Palladium Precatalysts for Cross-Coupling. *Nat. Rev. Chem.* **2017**, *1*, 0025.
- (18) Tobisu, M.; Chatani, N. Cross-Couplings Using Aryl Ethers via C-O Bond Activation Enabled by Nickel Catalysts. *Acc. Chem. Res.* **2015**, *48*, 1717-1726.
- (19) Wang, H.; Zhang, S. Q.; Hong, X. Computational Studies on Ni-Catalyzed Amide C-N Bond Activation. *Chem Commun.* **2019**, *55*, 11330-11341.
- (20) Shu, W.; Garcia-Dominguez, A.; Quiros, M. T.; Mondal, R.; Cardenas, D. J.; Nevado, C. Ni-Catalyzed Reductive Dicarbofunctionalization of Nonactivated Alkenes: Scope and Mechanistic Insights. *J. Am. Chem. Soc.* **2019**, *141*, 13812-13821.
- (21) Sun, S. Z.; Borjesson, M.; Martin-Montero, R.; Martin, R. Site-Selective Ni-Catalyzed Reductive Coupling of Alpha-Haloboranes with Unactivated Olefins. *J. Am. Chem. Soc.* **2018**, *140*, 12765-12769.
- (22) Zhu, C.; Liu, Z. Y.; Tang, L.; Zhang, H.; Zhang, Y. F.; Walsh, P. J.; Feng, C. Migratory Functionalization of Unactivated Alkyl bromides for Construction of All-Carbon Quaternary Centers via Transposed Tert-C-radicals. *Nat Commun* **2020**, *11*, 4860.
- (23) Derosa, J.; Tran, V. T.; Boulous, M. N.; Chen, J. S.; Engle, K. M. Nickel-Catalyzed Beta, Gamma-Dicarbofunctionalization of Alkenyl Carbonyl Compounds via Conjunctive Cross-Coupling. *J. Am. Chem. Soc.* **2017**, *139*, 10657-10660.
- (24) Derosa, J.; van der Puyl, V. A.; Tran, V. T.; Liu, M.; Engle, K. M. Directed Nickel-Catalyzed 1,2-Dialkylation of Alkenyl CarBonyl Compounds. *Chem Sci* **2018**, *9*, 5278-5283.
- (25) Dhungana, R. K.; Sapkota, R. R.; Wickham, L. M.; Niroula, D.; Giri, R. Ni-Catalyzed Regioselective 1,2-Dialkylation of Alkenes Enabled by the Formation of Two C(sp(3))-C(sp(3)) Bonds. *J. Am. Chem. Soc.* **2020**, *142*, 20930-20936.
- (26) Gu, J. W.; Min, Q. Q.; Yu, L. C.; Zhang, X. Tandem Difluoroalkylation-Arylation of Enamides Catalyzed by Nickel. *Angew. Chem. Int. Ed.* **2016**, *55*, 12270-12274.
- (27) Li, W.; Boon, J. K.; Zhao, Y. Nickel-catalyzed Difunctionalization of Allyl Moieties Using Organoboronic Acids and Halides with Divergent Regioselectivities. *Chem Sci* **2018**, *9*, 600-607.
- (28) Xu, C.; Yang, Z.-F.; An, L.; Zhang, X. Nickel-Catalyzed Difluoroalkylation—Alkylation of Enamides. *ACS Catal.* **2019**, *9*, 8224-8229.
- (29) Yang, T.; Chen, X.; Rao, W.; Koh, M. J. Broadly Applicable Directed Catalytic Reductive Difunctionalization of Alkenyl Carbonyl Compounds. *Chem* **2020**, *6*, 738-751.
- (30) Correa, A.; Leon, T.; Martin, R. Ni-catalyzed Carboxylation of C(sp2)- and C(sp3)-O Bonds with CO2. *J. Am. Chem. Soc.* **2014**, *136*, 1062-1069.
- (31) Haas, D.; Hammann, J. M.; Greiner, R.; Knochel, P. Recent Developments in Negishi Cross-Coupling Reactions. *ACS Catal.* **2016**, *6*, 1540-1552.
- (32) Takaya, J. Catalysis Using Transition Metal Complexes Featuring Main Group Metal and Metalloid Compounds as Supporting Ligands. *Chem Sci* **2021**, *12*, 1964-1981.

- (33) You, D.; Gabbaï, F. P. Tunable σ-Accepting, Z-Type Ligands for Organometallic Catalysis. *Trends Chem.* **2019**, *1*, 485-496.
- (34) González-Pérez, A. B.; Álvarez, R.; Faza, O. N.; de Lera, Á. R.; Aurrecoechea, J. M. DFT-Based Insights into Pd–Zn Cooperative Effects in Oxidative Addition and Reductive Elimination Processes Relevant to Negishi Cross-Couplings. *Organometallics* **2012**, *31*, 2053-2058.
- (35) Liberman-Martin, A. L.; Levine, D. S.; Ziegler, M. S.; Bergman, R. G.; Tilley, T. D. Lewis Acid-Base Interactions between Platinum(ii) Diaryl Complexes and Bis(perfluorophenyl)zinc: Strongly Accelerated Reductive Elimination Induced by A Z-Type Ligand. *Chem Commun*, **2016**, *52*, 7039-7042.
- (36) Mazzacano, T. J.; Mankad, N. P. Base Metal Catalysts For Photochemical C-H Borylation that Utilize Metal-Metal Cooperativity. *J. Am. Chem. Soc.* **2013**, *135*, 17258-17261.
- (37) Miloserdov, F. M.; Rajabi, N. A.; Lowe, J. P.; Mahon, M. F.; Macgregor, S. A.; Whittlesey, M. K. Zn-Promoted C-H Reductive Elimination and H2 Activation via a Dual Unsaturated HeteroBimetallic Ru-Zn Intermediate. *J. Am. Chem. Soc.* **2020**, *142*, 6340-6349.
- (38) Pell, C. J.; Shih, W. C.; Gatard, S.; Ozerov, O. V. Formation of (PNP)Rh Complexes Containing Covalent Rhodium-Zinc Bonds in Studies of Potential Rh-Catalysed Negishi Coupling. *Chem Commun.* **2017**, *53*, 6456-6459.
- (39) Day, C. S.; Somerville, R. J.; Martin, R. Deciphering the Dichotomy Exerted by Zn(II) in the Catalytic sp2 C—O bond Functionalization of Aryl Esters at the Molecular Level. *Nat Catal* **2021**, *4*, 124-133.
- (40) Li, Y.; Zou, L.; Bai, R.; Lan, Y. Ni(i)–Ni(iii) vs. Ni(ii)–Ni(iv): mechanistic study of Ni-Catalyzed Alkylation of Benzamides with Alkyl halides. *Org. Chem. Front.* **2018**, *5*, 615-622.
- (41) Zhang, T.; Liu, S.; Zhu, L.; Liu, F.; Zhong, K.; Zhang, Y.; Bai, R.; Lan, Y. Theoretical Study of FMO Adjusted C-H Cleavage and Oxidative Addition in Nickel Catalysed C-H Arylation. *Commun Chem.* **2019**, *2*, 31.
- (42) Li, Y.; Luo, Y.; Peng, L.; Li, Y.; Zhao, B.; Wang, W.; Pang, H.; Deng, Y.; Bai, R.; Lan, Y.; Yin, G. Reaction Scope and Mechanistic Insights of Nickel-catalyzed Migratory Suzuki-Miyaura Cross-Coupling. *Nat Commun* **2020**, *11*, 417.
- (43) Frisch, M. J. T., G. W.; Schlegel, H. B.; Scuseria, G. E.;; Robb, M. A. C., J. R.; Scalmani, G.; Barone, V.; Mennucci,; B.; Petersson, G. A. N., H.; Caricato, M.; Li, X.; Hratchian, H.; P.; Izmaylov, A. F. B., J.; Zheng, G.; Sonnenberg, J. L.; Hada, M.;; Ehara, M. T., K.; Fukuda, R.; Hasegawa, J.; Ishida, M.; Nakajima,; T.; Honda, Y. K., O.; Nakai, H.; Vreven, T.; Montgomery, J. A., Jr.;; Peralta, J. E. O., F.; Bearpark, M.; Heyd, J. J.; Brothers, E.; Kudin,; K. N.; Staroverov, V. N. K., R.; Normand, J.; Raghavachari, K.;; Rendell, A. B., J. C.; Iyengar, S. S.; Tomasi, J.; Cossi, M.; Rega,; N.; Millam, J. M. K., M.; Knox, J. E.; Cross, J. B.; Bakken, V.;; Adamo, C. J., J.; Gomperts, R.; Stratmann, R. E.; Yazyev, O.;; Austin, A. J. C., R.; Pomelli, C.; Ochterski, J. W.; Martin, R. L.;; Morokuma, K. Z., V. G.; Voth, G. A.; Salvador, P.;; Dannenberg, J. J. D., S.; Daniels, A. D.; Farkas, O.;; Foresman, J. B. O., J. V.; Cioslowski, J.; Fox, D. J. Gaussian 09,; revision D.01; Gaussian, I. W., CT, 2009.

- (44) Becke, A. D. Density Functional Thermochemistry. III. The Role of Exact Exchange. *J. Chem. Phys* **1993**, *98*, 5648-5652.
- (45) Lee, C.; Yang, W.; Parr, R. G. Development of the Colle-Salvetti Correlation-Energy Formula into A Functional of the Electron Density. *Phys. Rev. B* **1988**, *37*, 785-789.
- (46) Li, Z. Q.; Apolinar, O.; Deng, R.; Engle, K. M. Directed Markovnikov hydroarylation and hydroalkenylation of alkenes under nickel catalysis. *Chem. Sci.* **2021**, *12*, 11038-11044.
- (47) Liu, S.; Qi, X.; Bai, R.; Lan, Y. Theoretical Study of Ni-Catalyzed C-N Radical-Radical Cross-Coupling. *J. Org. Chem.* **2019**, *84*, 3321-3327.
- (48) Zhao, Y.; Truhlar, D. G. The M06 Suite of Density Functionals for Main Group Thermochemistry, Thermochemical Kinetics, Noncovalent Interactions, Excited States, and Transition Elements: Two New Functionals and Systematic Testing of Four M06-Class Functionals and 12 Other Functionals. *Theor. Chem. Acc.* 2007, 120, 215-241.
- (49) Zhao, Y.; Truhlar, D. G. Density Functionals with Broad Applicability in Chemistry. *Acc. Chem. Res.* **2008**, *41*, 157-167.
- (50) Chen, H.; Zhu, L.; Zhong, K.; Yue, X.; Qu, L.-B.; Bai, R.; Lan, Y. Theoretical insight into phosphoric acid-catalyzed asymmetric conjugate addition of indolizines to α,β-unsaturated ketones. *Chinese Chem Lett.* **2018**, *29*, 1237-1241.
- (51) Lin, Y. S.; Tsai, C. W.; Li, G. D.; Chai, J. D. Long-Range Corrected Hybrid Meta-Generalized-Gradient Approximations with Dispersion Corrections. *J. Chem. Phys.* **2012**, *136*, 154109.
- (52) Peverati, R.; Truhlar, D. G. Performance of the M11 and M11-L Density Functionals for Calculations of Electronic Excitation Energies by Adiabatic Time-Dependent Density Functional Theory. *Phys. Chem. Chem. Phys.* **2012**, *14*, 11363-11370.
- (53) Steckel, J. A. Ab Initio Calculations of the Interaction between CO2 and the Acetate Ion. *J. Phys. Chem. A* **2012**, *116*, 11643-11650.
- (54) Zhao, Y.; Ng, H. T.; Peverati, R.; Truhlar, D. G. Benchmark Database for Ylidic Bond Dissociation Energies and Its Use for Assessments of Electronic Structure Methods. *J. Chem. Theory. Comput.* **2012**, *8*, 2824-2834.
- (55) Cancès, E.; Mennucci, B.; Tomasi, J. A new Integral Equation Formalism for the Polarizable Continuum Model: Theoretical Background and Applications to Isotropic and Anisotropic Dielectrics. *J. Chem. Phys.* **1997**, *107*, 3032-3041.
- (56) Cossi, M.; Barone, V.; Cammi, R.; Tomasi, J. Ab Initio Study of Solvated Molecules: A new implementation of the Polarizable Continuum Model. *Chem. Phys. Lett.* **1996**, *255*, 327-335.
- (57) Zhu, S.; Zhao, X.; Li, H.; Chu, L. Catalytic Three-Component Dicarbofunctionalization Reactions Involving Radical Capture by Nickel. *Chem. Soc. Rev.* **2021**, *50*, 10836-10856.
- (58) Tran, V. T.; Li, Z. Q.; Gallagher, T. J.; Derosa, J.; Liu, P.; Engle, K. M. Integrating Allyl Electrophiles into Nickel-Catalyzed Conjunctive Cross-Coupling. *Angew. Chem. Int. Ed.* **2020**, *59*, 7029-7034.

